2

High Lattice Thermal Conductivity Solids

Donald T. Morelli and Glen A. Slack

The lattice thermal conductivity κ of various classes of crystalline solids is reviewed, with emphasis on materials with $\kappa > 0.5\,\mathrm{Wcm^{-1}K^{-1}}$. A simple model for the magnitude of the lattice thermal conductivity at temperatures near the Debye temperature is presented and compared to experimental data on rocksalt, zincblende, diamond, and wurtzite structure compounds, graphite, silicon nitride and related materials, and icosahedral boron compounds. The thermal conductivity of wide-band-gap Group IV and Group III–V semiconductors is discussed, and the enhancement of lattice thermal conductivity by isotopic enrichment is considered.

2.1 Introduction: The Importance of Thermal Conductivity

A solid's thermal conductivity is one of its most fundamental and important physical parameters. Its manipulation and control have impacted an enormous variety of technical applications, including thermal management of mechanical, electrical, chemical, and nuclear systems; thermal barriers and thermal insulation materials; more efficient thermoelectric materials; and sensors and transducers. On a more fundamental level, the study of the underlying physics of the heat-conduction process has provided a deep and detailed understanding of the nature of lattice vibrations in solids. In this review we focus on solid electrically insulating materials with high lattice thermal conductivity. By lattice thermal conductivity we mean heat conduction via vibrations of the lattice ions in a solid. Our goal is to first provide a simple physical picture for lattice heat conduction in solids and to then compare this model with experimental data on the thermal conductivity of several classes of crystal structures and types of materials. The review is similar in spirit to that of Slack [1] but incorporates and discusses data and experimental results that have been obtained since that review. The present work is mainly concerned with the intrinsic lattice thermal conductivity of solids. Klemens [2] has reviewed the influence of various types of defects and impurities on the lattice

thermal conductivity. The classic monograph of Berman [3] discusses all aspects of the thermal conductivity of solids, including metals, polymers, and amorphous materials. A more recent update on materials advances in the area of high thermal conductivity has also recently appeared in the literature [4].

The fact that certain materials that are good electrical insulators can possess high thermal conductivity is frequently met with surprise and puzzlement by the casual observer. This is easily understood, however, when one realizes that whereas electrical current in a material is carried solely by charge carriers, heat may be transported by both charge carriers and vibrations of the lattice ions. In a good metal like copper, the electron density is large, and nearly all of the heat conduction occurs via charge carrier transport. This electronic thermal conductivity masks the lattice thermal conductivity, which is present but small relative to the electronic term. In a material where there are no free electrons to carry heat, the lattice thermal conductivity is the only mode of heat transport available. Within the family of electrically insulating materials, the magnitude of the lattice thermal conductivity, κ, can vary over an extremely wide range. For instance, diamond has a thermal conductivity at room temperature of $30\,\mathrm{Wcm^{-1}K^{-1}}$, much higher than that of any material, including the best metals. On the other hand, some polymeric materials and amorphous electrically insulating solids have thermal conductivity at room temperature as low as $0.001\,\mathrm{Wcm^{-1}K^{-1}}$. We want to understand why certain materials can possess high lattice thermal conductivity and what physical mechanisms serve to provide a limit to the lattice thermal conductivity of solids.

The review is organized as follows. In Sect. 2.2 we will introduce simple models of lattice heat conduction that can be used to predict the magnitude and temperature dependence of the thermal conductivity. In Sect. 2.3 we consider some specific classes of materials that possess high thermal conductivity and compare experimental results with the predictions of this model. Sect. 2.4 takes a closer look at lattice heat conduction in several technologically important wide-band-gap semiconductors. In Sect. 2.5 we discuss how the isotope effect may be used to increase the lattice thermal conductivity of some materials. Finally, Sect. 2.6 provides a summary and suggests some future directions of research on high-thermal-conductivity solids.

Of course we must first define what we mean by "high" thermal conductivity. As mentioned previously, the lattice thermal conductivity of solids near ambient temperature can span an enormously wide range. "High" thermal conductivity is thus a relative term; for instance, a polymer with a thermal conductivity of $0.03\,\mathrm{Wcm^{-1}K^{-1}}$ would, for this class of solids, have a "high" thermal conductivity. On the other hand, such a value of thermal conductivity for an inorganic crystalline semiconductor (the thermoelectric material PbTe, for example) would be considered very "low". Frequently in the literature a value of thermal conductivity in excess of $1\,\mathrm{Wcm^{-1}K^{-1}}$ has been chosen, rather arbitrarily, as the lower limit for a high-thermal-conductivity solid. Because the main driver in the search for high-thermal-conductivity solids is

for thermal management of electronics systems, a more suitable metric may be how the thermal conductivity compares to traditional materials used in these types of applications. By far the most widely used material for thermal management in high-volume applications is crystalline alumina, with a thermal conductivity on the order of $0.5\,\mathrm{Wcm^{-1}K^{-1}}$. We will thus set our lower limit for "high" thermal conductivity at $0.5\,\mathrm{Wcm^{-1}K^{-1}}$. As we shall see, even with this more relaxed criterion, the family of high-thermal-conductivity electrical insulators is still rather small.

2.2 Simple Model of the Magnitude of Lattice Heat Conduction in Solids

2.2.1 Normal Modes of Vibrations of a Lattice

The concepts central to an understanding of the lattice thermal conductivity of a solid are captured in the simple model of a linear chain of atoms of mass M held together by springs of force constant k. If the rest of the atoms are a distance a apart, the relation between the frequency ω and wavenumber q of a wave along the chain is given by

$$\omega(q) = 2\sqrt{\frac{k}{M}}|\sin(qa/2)|. \tag{2.1}$$

This relationship between the frequency and wavenumber of a wave is termed the dispersion curve and is illustrated in Fig. 2.1a for wavenumber ranging between $-\pi/\mathrm{a}$ and $+\pi/\mathrm{a}$, which represents the first Brillouin zone for the one-dimensional chain in reciprocal space. An essential feature of the relationship between frequency and wavenumber that distinguishes the present case from that of a continuum elastic wave is the bending over, or "dispersion," of the curve near the edge of the Brillouin zone. Because the group velocity of the wave is given by $\mathrm{v} = d\omega/dq$, near these extrema the velocity of the wave tends to zero.

In a linear chain of atoms with two different types of masses, M_1 and M_2, alternating along the length of the chain, there are two solutions to the wave equation, and the resulting $\omega - q$ relations are termed the two branches of the dispersion relation. These are shown in Fig. 2.1(b). The lower branch, called the acoustic branch because the linear relationship $\omega = \mathrm{v}q$ for low frequency is similar to that for a sound wave, is the same as that for the case of a chain of atoms of a single type, shown in Fig. 2.1(a). This branch corresponds to two neighboring atoms moving in phase with one another. The upper branch,

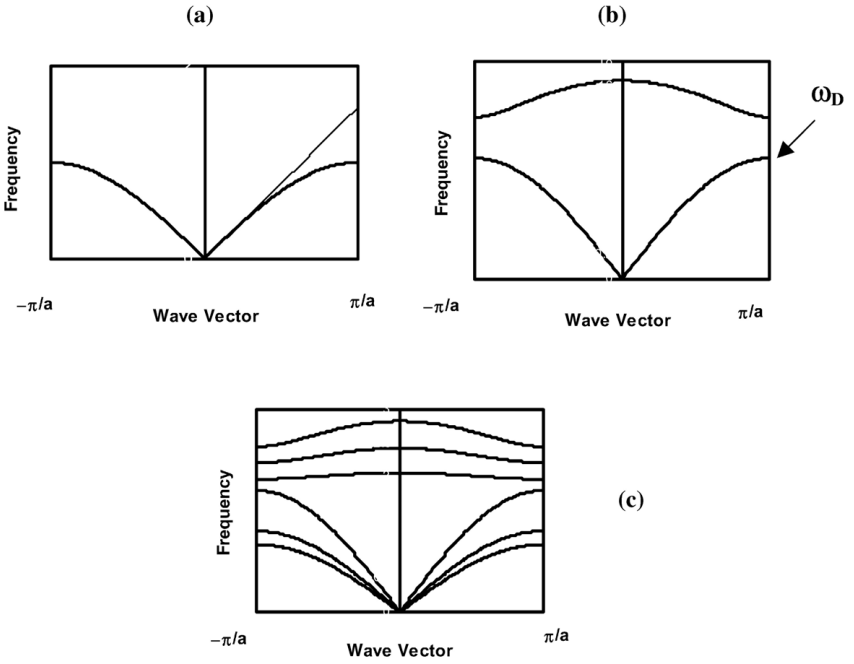

Fig. 2.1. Models of phonon-dispersion curves for solids: (a) one-dimensional case for single-atom type spaced by distance a, fine line represents continuum case; (b) one-dimensional case for two atoms with differing masses, showing the occurrence of both an acoustic (lower curve) and an optic (upper curve) branch; ω_D, where the acoustic branch meets the zone edge, is the Debye frequency for the acoustic phonons; (c) three-dimensional lattice with two different atom masses.

called the optic branch, corresponds to the case where two neighboring atoms are moving out of phase with one another; for low frequencies this branch is characterized by a vanishing group velocity. Because the group velocity of the optic branch is small, these modes generally do not participate in the heat transport process, and most of the energy transport along the chain occurs via the acoustic branch. This is a basic assumption that we use throughout this review. There are instances, however, especially at high temperatures, when this may not be true; these are touched on in Sect. 2.3. Possible heat conduction by optic phonons is considered in more detail in the review by Slack [1] and has been treated for the specific case of alkali halide compounds by Pettersson [5]. Additionally, while the optic branch is generally ineffective in transporting heat, these modes may "interact" with the heat-carrying acoustic vibrations and thus can be important in determining the magnitude of the thermal conductivity.

Of course, an actual crystal is not a linear chain of atoms but a three-dimensional lattice. In this case, if all the atoms of the lattice are

of the same mass, there are three acoustic branches representing the three polarization modes (one longitudinal and two transverse) of the crystal. If there is more than one type of atom per unit cell, the dispersion relation again will contain optic modes. As in the one-dimensional case, these modes are typified by high frequency and low group velocity. The dispersion curve for a three-dimensional lattice containing two different types of atoms is shown in Fig. 2.1(c). For the more general case of N types of atoms, there will be three acoustic branches and $3(N-1)$ optic branches.

Of fundamental importance in the heat transport in a lattice is the concept of the Debye frequency, ω_D, which is defined here as the maximum vibrational frequency of a given mode in a crystal. For acoustic modes, this corresponds to the frequency at the zone boundary as indicated in Fig. 2.1(b) for the one-dimensional chain. One can define a Debye temperature θ_a for an acoustic phonon branch as:

$$\theta_a = \frac{\hbar\omega_D}{k_B}, \tag{2.2}$$

where $\hbar$ is the Planck constant and k_B is the Boltzmann constant. For the three-dimensional case each acoustic branch will have a Debye temperature given by Eq. (2.2) with its appropriate value of ω_D.

An alternative method of calculating θ_a is by integrating the acoustic portion of the phonon density of states $g(\omega)$ over the Brillouin zone according to [6]:

$$\theta_a^2 = \frac{5\hbar^2}{3k_B^2} \frac{\int_0^{\omega_D} \omega^2 g(\omega) d\omega}{\int_0^{\omega_D} g(\omega) d\omega}. \tag{2.3}$$

For $g(\omega) \sim \omega^2$ these two definitions are equivalent. The Debye temperature can be thought of as the temperature above which all vibrational modes in a crystal are excited.

Clearly, given the dispersion relations of real crystals, the Debye temperature for heat transport is determined by where the acoustic branches of the vibrational spectrum meet the Brillouin zone edge; this will be different from the Debye temperature determined by other means, such as calculation from the elastic constants or from the low-temperature specific heat. The importance of this point has been discussed in detail by Slack [1] and will become clearer as our discussion continues.

Although the preceding discussion is useful for describing the frequency–wave vector relationships for phonons, it is insufficient for a discussion of the thermal conductivity. This is because in the presence of only harmonic interactions there is no means of interaction between different phonons, and in such a situation the mean free path for lattice vibrations would be infinite. Only by considering the higher-order anharmonic terms in the ionic interaction energy

can we account for finite thermal conductivity. These higher-order terms are characterized by the Grüneisen constant γ. This "constant" is defined as the rate of change of the vibrational frequency of a given mode with volume:

$$\gamma = -\frac{d \ln \omega_i}{d \ln V} \tag{2.4}$$

and is therefore not a constant but a function of q. Again, different vibrational modes will have different values of γ. Because γ is a measure of the departure of a crystal from harmonicity, we expect that any model of the thermal conductivity will include this parameter as well. What we really want are the γ-values for the acoustic modes at temperatures on the order of the Debye temperature, which unfortunately are unavailable in most circumstances. The γ-values determined from thermal expansion data, for instance, average over all phonon branches, including the optic branches. Thus there is a great deal of uncertainty in the choice of this parameter for many of the solids we are considering in this review. Recently some lattice dynamical calculations have become available that provide mode Grüneisen parameters, and we will use these in estimating γ-values when appropriate. In other cases γ will be estimated from thermal expansion data.

2.2.2 Normal and Umklapp Phonon-Scattering Processes

Even in a perfect crystal there are interactions of phonons among themselves that tend to restore the phonon distribution to equilibrium. The interactions that give rise to thermal resistance involve powers higher than quadratic in the perturbation Hamiltonian describing the potential energy of a displaced ion in the lattice. Terms that are cubic in the displacement can be thought of as arising from three-phonon interactions, while those that are quartic arise from interactions among four phonons. Let us for simplicity consider only the cubic anharmonic term involving modes (ω_1, q_1) and (ω_2, q_2) interacting and resulting in mode (ω_3, q_3). The transition probability for the three-phonon process giving rise to this term is nonzero only if:

$$\omega_1 + \omega_2 = \omega_3 \quad \text{and} \quad q_1 + q_2 = q_3 + K, \tag{2.5}$$

where K is equal to zero for a so-called normal phonon process and equal to a reciprocal lattice vector for a so-called Umklapp process. This latter process, from the German phrase "to flip over," represents a situation in which the net phonon flux is reversed in direction. It can be shown that only Umklapp processes give rise to thermal resistance, and as a first approximation one can ignore the existence of normal processes in determining the thermal conductivity.

2.2.3 Relaxation-Time Approximation

In the *relaxation-time approximation* [3], it is assumed that the phonon distribution is restored to the equilibrium distribution at a rate proportional to the departure from equilibrium. By assuming a linear dispersion relation, the thermal conductivity can be expressed as:

$$\kappa_L = \frac{k_B}{2\pi^2 v}\left(\frac{k_B T}{\hbar}\right)^3 \int_0^{\theta_D/T} \frac{x^4 e^x}{\tau_C^{-1}(e^x-1)^2} dx, \tag{2.6}$$

where $x = \hbar\omega/k_B T$ is dimensionless, ω is the phonon frequency, k_B is the Boltzmann constant, $\hbar$ is the Planck constant, θ_D is the Debye temperature, v is the velocity of sound, and τ_C is the total phonon-scattering relaxation time. The various processes that scatter phonons are assumed to be independent of one another and to be described by individual scattering rates τ_i^{-1} such that:

$$\tau_c^{-1} = \sum_i \tau_i^{-1}. \tag{2.7}$$

In general, the various scattering processes i will depend on both temperature and phonon frequency. In addition to the intrinsic Umklapp scattering process, a wide variety of other types of phonon-scattering mechanisms, including boundary scattering, point defect scattering, dislocation scattering, and magnetic scattering, to name just a few, have been considered in the literature; these are discussed in more detail in earlier reviews. Some of these scattering processes will be considered in more detail later.

2.2.4 Callaway Model

While it is indeed true that normal processes themselves do not give rise to thermal resistance, it is incorrect to assume that they do not influence the thermal conductivity, because they are capable of redistributing momentum and energy among phonons that are more likely to undergo a resistive scattering process. The most widely accepted model describing this process is that of Callaway [7]. In the Callaway model, the thermal conductivity is composed of two terms:

$$\kappa = \kappa_1 + \kappa_2$$

with

$$\kappa_1 = \frac{1}{3} C T^3 \int_0^{\theta/T} \frac{\tau_c(x) x^4 e^x}{(e^x-1)^2}\, dx$$

and

$$\kappa_2 = \frac{1}{3} C T^3 \frac{\left[\int_0^{\theta/T} \frac{\tau_c(x) x^4 e^x}{\tau_N(x)(e^x-1)^2}\, dx \right]^2}{\int_0^{\theta_L/T} \frac{\tau_c(x) x^4 e^x}{\tau_N(x)\tau_R(x)(e^x-1)^2}\, dx}. \tag{2.8}$$

In these expressions, τ_R represents the scattering time due to resistive processes, τ_N the scattering time due to normal phonon processes, and $\tau_c^{-1} = \tau_R^{-1} + \tau_N^{-1}$ represents the combined scattering rate. We shall see that in some circumstances an adequate description of the thermal conductivity can be obtained using (2.6) while in others it is necessary to take into account normal phonon-scattering processes.

2.2.5 Thermal Conductivity Near the Debye Temperature

We see that a comprehensive model for the lattice thermal conductivity of a solid requires not only knowledge of the phonon spectrum and Grüneisen parameters, but also an understanding of various types of phonon-scattering rates and their temperature and frequency dependencies. Now we will concern ourselves only with an understanding of the intrinsic thermal conductivity of a solid in a temperature range where only interactions among the phonons themselves via anharmonic Umklapp processes are important. Various early estimates of the lattice thermal conductivity of a solid in this regime have been discussed by Slack [1] and Berman [3], and can be considered for our purposes as approximate expressions for the thermal conductivity at temperatures not too far removed from the Debye temperature of the solid. These estimates all take the form

$$\kappa = A \cdot \frac{M_a \theta_a^3 \delta}{\gamma^2 T}, \tag{2.9}$$

where M_a is the atomic mass of the atom, δ^3 is the volume per atom, and A is a constant. Leibfried and Schlömann [8] give the constant as $A = 5.72 \times 10^{-8}$ for δ in Angstroms and M_a in atomic mass units. Julian [9] pointed out an error in their calculation and determined the following value for A:

$$A = \frac{2.43 \cdot 10^{-8}}{1 - 0.514/\gamma + 0.228/\gamma^2}. \tag{2.10}$$

Slack [1] put $\gamma \approx 2$ in this expression and used $A = 3.04 \times 10^{-8}$. The γ-dependence of A is slight and we will allow this parameter to assume its value appropriate to the value of γ used to calculate the thermal conductivity.

2.2.6 Extension to More Complex Crystal Structures and Criteria for High Thermal Conductivity

Equation (2.9) is valid for structures containing only one atom per primitive unit cell. Using a simple counting scheme, Slack [1] extended the model to

crystals with n atoms per unit cell:

$$\kappa = A \cdot \frac{\overline{M}_a \theta_a^3 \delta n^{1/3}}{\gamma^2 T}. \tag{2.11}$$

By using the Debye temperature appropriate for the acoustic modes only, this equation is a quantitative statement of our basic assumption that the optic modes in crystals with $n > 1$ do not contribute to the heat transport process.

In many circumstances, especially in considering new materials and crystal structures, the phonon-dispersion relations used to calculate θ_a are not available either experimentally or theoretically. In these cases, the acoustic-mode Debye temperature can be determined from the "traditional" definition of the Debye temperature θ (namely that determined from the elastic constants or specific heat) by using [10]

$$\theta_a = \theta n^{-1/3}. \tag{2.12}$$

With increasing n, the size of the unit cell (that is, the lattice constant a) in real space increases. This means that the Brillouin zone boundary (see Fig. 2.1) moves inward, thus cutting off phonon frequencies at smaller values as n increases. The "traditional" Debye temperature θ depends on the atomic mass and the bond strength but is independent of n. Thus Eq. (2.11) can be rewritten to display the explicit n-dependence of the thermal conductivity as:

$$\kappa = A \cdot \frac{\overline{M} \theta^3 \delta}{\gamma^2 T n^{2/3}}. \tag{2.13}$$

On the basis of Eq. (2.13) we may now list the necessary criteria for an electrically insulating solid to possess high thermal conductivity:

- high Debye temperature,
- small Grüneisen parameter, and
- small n (simple crystal structure).

2.3 Materials with High Lattice Thermal Conductivity

2.3.1 Rocksalt, Diamond, and Zincblende Crystal Structures

We can test the validity of this simple model for thermal conductivity by comparing it to experimental data. Let us begin by considering classes of solids with common values of n. The only nonmetallic crystals with $n = 1$ are the rare gas crystals, which crystallize in the simple cubic structure. These crystals, however, all have Debye temperatures less than 100 K, and as a result, have $\kappa < 0.5\,\mathrm{Wcm^{-1}K^{-1}}$ and will not be considered further.

The families of crystals with $n = 2$ include the rocksalt, diamond, and zincblende structure compounds. The main members of these three families that we will consider here are shown in Tables 2.1 and 2.2, respectively, along

Table 2.1. Calculated and experimental room-temperature thermal conductivity of several rocksalt ($n = 2$) compounds. θ_a = high-temperature Debye temperature of the acoustic phonon branch; γ = high-temperature Grüneisen constant; δ^3 = volume per atom; M = average atomic mass; κ_{calc} = calculated thermal conductivity from equation (2.13); κ_{exp} = measured thermal conductivity.

Compound	θ_a (K)	γ	δ (Å)	M (amu)	κ_{calc} ($\text{Wcm}^{-1}\text{K}^{-1}$)	κ_{exp} ($\text{Wcm}^{-1}\text{K}^{-1}$)
LiH	615	1.28	2.04	3.97	0.159	0.15
LiF	500	1.5	2.00	12.97	0.194	0.176
NaF	395	1.5	2.31	21.00	0.179	0.184
NaCl	220	1.56	2.81	29.22	0.048	0.071
NaBr	150	1.5	2.98	51.45	0.031	0.028
NaI	100	1.56	3.23	74.95	0.013	0.018
KF	235	1.52	2.66	2.05	0.058	
KCl	172	1.45	3.14	37.27	0.038	0.071
KBr	117	1.45	3.30	59.50	0.020	0.034
KI	87	1.45	3.52	68.00	0.010	0.026
RbCl	124	1.45	3.27	60.46	0.024	0.028
RbBr	105	1.45	3.42	82.69	0.021	0.038
RbI	84	1.41	3.66	106.10	0.015	0.023
MgO	600	1.44	2.11	20.00	0.596	0.6
CaO	450	1.57	2.4	28.04	0.332	0.27
SrO	270	1.52	2.57	51.81	0.152	0.12
BaO	183	1.5	2.7	76.66	0.076	0.023
PbS	115	2	2.97	119.60	0.017	0.029
PbSe	100	1.5	3.06	143.08	0.035	0.020
PbTe	105	1.45	3.23	167.4	0.040	0.025

with the parameters needed to calculate their thermal conductivities using Eq. (2.13).

Let us consider the rocksalt compounds first; see Table 2.1. Here the Debye temperatures for acoustic phonons have been determined either from Eq. (2.2) or (2.3); in cases where both the phonon density of states and the phonon-dispersion relations are available, the calculated Debye temperatures using these two methods differ by less than 10 percent. For the Grüneisen parameters we use the data collected by Slack [1]. It should be noted that there is remarkably little variation in the γs for these rocksalts, with the majority of them lying in the range 1.5–1.9.

Figure 2.2 is a plot of the measured thermal conductivity at room temperature as a function of the calculated thermal conductivity. We see that, with data spanning a range of two orders of magnitude, Eq. (2.13) actually gives a very good description of the thermal conductivity of the rocksalt compounds. The tendency for the measured thermal-conductivity values to exceed the calculated ones has been attributed to a contribution from optic phonons. According to the criterion introduced earlier, only one rocksalt

Table 2.2. Calculated and experimental room-temperature thermal conductivity of several zincblende and diamond structure ($n = 2$) compounds. θ_a = high-temperature Debye temperature of the acoustic phonon branch; γ = high-temperature Grüneisen constant; δ^3 = volume per atom; M = average atomic mass; $\kappa_{\rm calc}$ = calculated thermal conductivity from Eq. (2.13); $\kappa_{\rm exp}$ = measured thermal conductivity.

Element/ Compound	θ_a (K)	γ	δ (Å)	M (amu)	$\kappa_{\rm calc}$ ($\rm Wcm^{-1}K^{-1}$)	$\kappa_{\rm exp}$ ($\rm Wcm^{-1}K^{-1}$)
C	1450	0.75	1.78	12.01	16.4	30
Si	395	1.06	2.71	28.08	1.71	1.66
Ge	235	1.06	2.82	72.59	0.97	0.65
BN	1200	0.7	1.81	12.41	11.05	7.6
BP	670	0.75	2.27	20.89	3.59	3.5
BAs	404	0.75	2.39	42.87	1.70	
AlP	381	0.75	2.73	28.98	1.10	
AlAs	270	0.66	2.83	50.95	0.89	0.98
AlSb	210	0.6	3.07	74.37	0.77	0.56
GaP	275	0.75	2.73	50.35	0.72	1.00
GaAs	220	0.75	2.83	72.32	0.55	0.45
GaSb	165	0.75	3.05	95.73	0.33	0.4
InP	220	0.6	2.94	72.90	0.83	0.93
InAs	165	0.57	3.03	94.87	0.51	0.3
InSb	135	0.56	3.24	118.29	0.38	0.2
ZnS	230	0.75	2.71	48.72	0.40	0.27
ZnSe	190	0.75	2.84	72.17	0.35	0.19
ZnTe	155	0.97	3.05	96.49	0.17	0.18
CdSe	130	0.6	3.06	95.68	0.23	
CdTe	120	0.52	3.23	120.00	0.296	0.075

structure compound, MgO, can be categorized as a high-thermal-conductivity compound, with $\kappa \approx 0.6\,\rm Wcm^{-1}K^{-1}$ at room temperature.

We turn next to the zincblende and diamond structure compounds; see Table 2.2. One very striking feature of these compounds is that the Grüneisen parameters tend to be much lower than those of the rocksalt structure compounds: in the zincblende and diamond structures the phonons are more harmonic. In fact, for some members of this family, e.g., silicon, some of the mode Grüneisen parameters are negative [11]. Recent lattice dynamics calculations of the mode Grüneisen parameters for diamond, silicon, and boron nitride have been carried out [11, 12, 13]; see Fig. 2.3. Here we clearly see that the longitudinal modes tend to have Grüneisen parameters near unity, and the transverse modes have smaller, and even negative, γs. Of course the important parameter is the average value of the square of γ, and this is indicated in the figures. We see that the resulting average γs for these zincblende and diamond structure compounds as derived from lattice dynamics calculations are consistent with those presented in Table 2.2, which in most cases

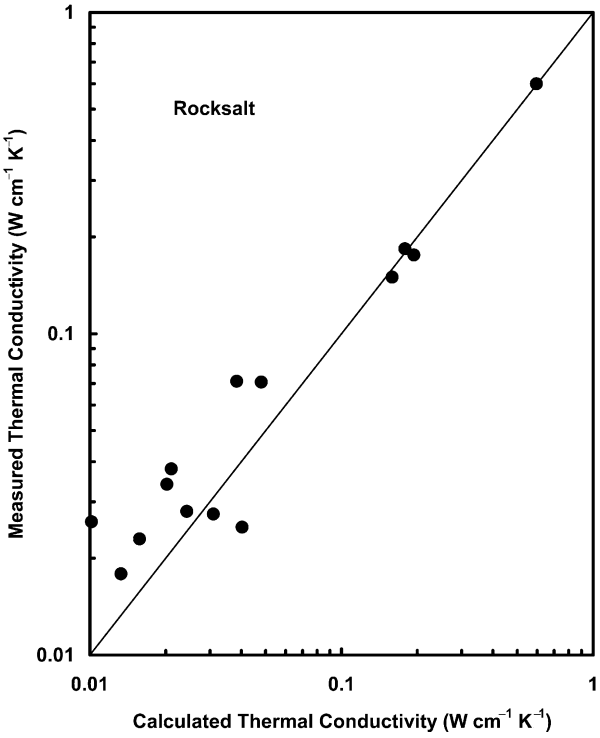

Fig. 2.2. Room-temperature thermal conductivity for the rocksalt compounds of Table 2.1 plotted against the thermal conductivity calculated from Eq. (2.13).

were derived from high-temperature thermal expansion data [1]. The necessity of a low γ for high-thermal conductivity is a recurring theme in this review. We see in Fig. 2.4 a very well-behaved relationship between measured and calculated room-temperature lattice thermal conductivities, spanning a range from $0.18\,\mathrm{Wcm^{-1}K^{-1}}$ for ZnTe to $>30\,\mathrm{Wcm^{-1}K^{-1}}$ for isotopically enriched diamond. Twelve members of this family of materials have or are expected to have thermal conductivity at room temperature in excess of $0.5\,\mathrm{Wcm^{-1}K^{-1}}$ with several (diamond, BN, BP, Si, BAs, AlP, and GaP) exceeding $1\,\mathrm{Wcm^{-1}K^{-1}}$. A more detailed description of the thermal conductivity of diamond is the subject of Chapter 7 in this book.

2.3.2 Wurtzite Crystal Structure

For the $n = 4$ wurtzite structure compounds CdS, ZnO, GaN, BeO, AlN, and SiC (Table 2.3 and Fig. 2.5) we again find excellent agreement between the calculated and measured room-temperature thermal conductivities, except

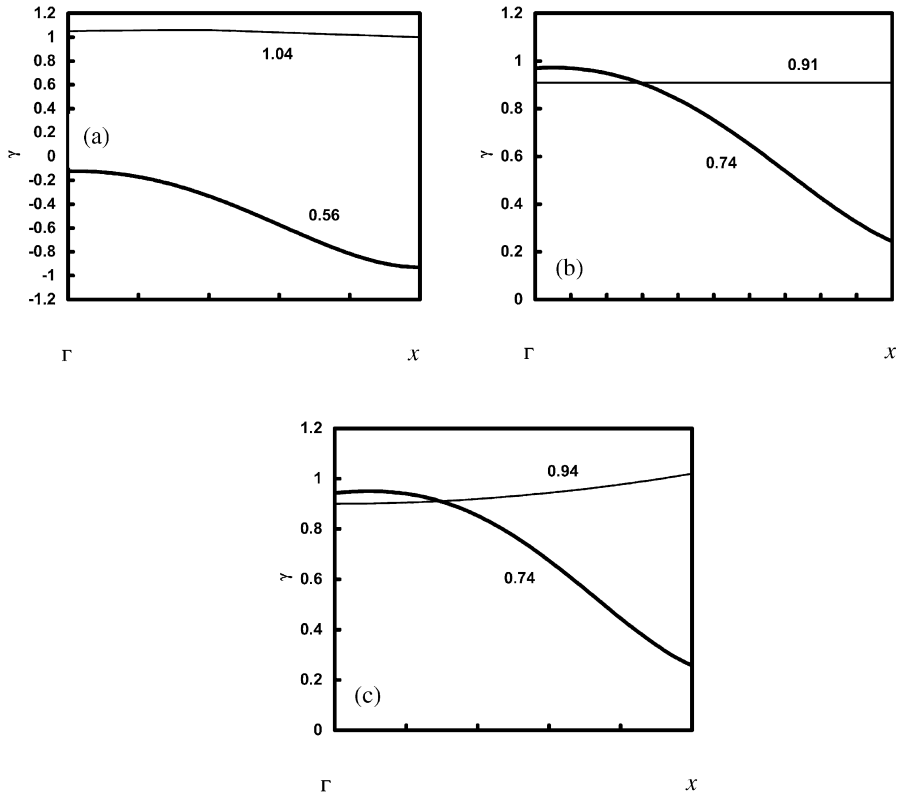

Fig. 2.3. Longitudinal (thin lines) and transverse (bold lines) mode Grüneisen parameters for (a) silicon, (b) diamond, and (c) boron nitride, with the average value $\langle \gamma_i^2 \rangle$ as indicated.

for the case of BeO, where the measured thermal conductivity exceeds the calculated value by about a factor of four. We note, however, that the value of $\gamma = 1.3$, which was derived from thermal expansion data [14], is significantly larger than that used for the other wurtzite compounds. Using a similar value of $\gamma = 0.75$ for BeO, in fact, improves greatly the agreement between the model and experiment. Further measurements or calculations of the Grüneisen parameter for BeO would be desirable. We note further that all of these compounds except CdS can be categorized as possessing high thermal conductivity according to our criterion. These crystals are undergoing significant development for their potentially useful electronic and optical properties; thus the last decade has seen a dramatic improvement in the availability and quality of single crystals of these wurtzites. Because of their technological potential, we will discuss the thermal conductivity of some of these crystals in more detail in Sect. 2.4.

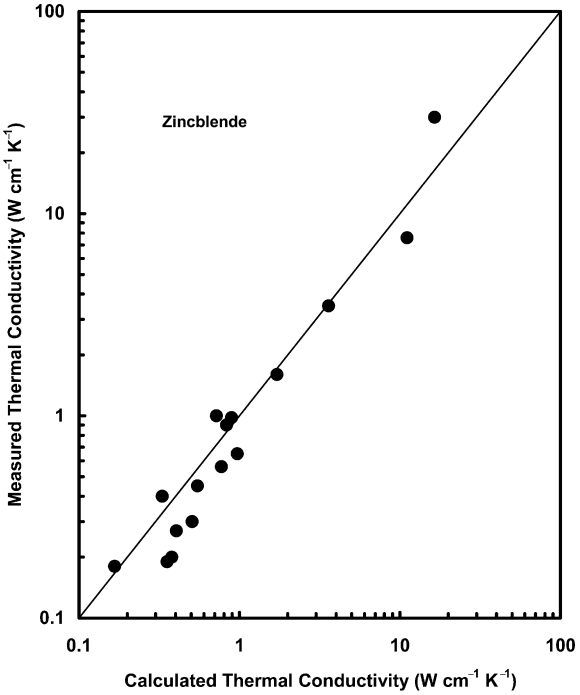

Fig. 2.4. Room-temperature thermal conductivity for the zincblende compounds of Table 2.2 plotted against the thermal conductivity calculated from Eq. (2.13).

Table 2.3. Calculated and experimental room-temperature thermal conductivity of several wurtzite ($n = 4$) compounds. θ_a = high-temperature Debye temperature of the acoustic phonon branch; γ = high-temperature Grüneisen constant; δ^3 = volume per atom; M = average atomic mass; $\kappa_{\rm calc}$ = calculated thermal conductivity from equation (2.13); $\kappa_{\rm exp}$ = measured thermal conductivity.

Compound	θ_a (K)	γ	δ (Å)	M (amu)	$\kappa_{\rm calc}$ ($\rm Wcm^{-1}K^{-1}$)	$\kappa_{\rm exp}$ ($\rm Wcm^{-1}K^{-1}$)
SiC	740	0.75	2.18	20.0	4.45	4.9
AlN	620	0.7	2.18	20.49	3.03	3.5
GaN	390	0.7	2.25	41.87	1.59	2.1
ZnO	303	0.75	2.29	40.69	0.65	0.6
BeO	809	1.38/0.75	1.90	12.51	0.90/3.17	3.7
CdS	135	0.75	2.92	72.23	0.13	0.16

2.3.3 Silicon Nitride and Related Structures

Up to now we have discussed structures containing only two or four atoms per primitive unit cell. We will now consider briefly a few compounds with

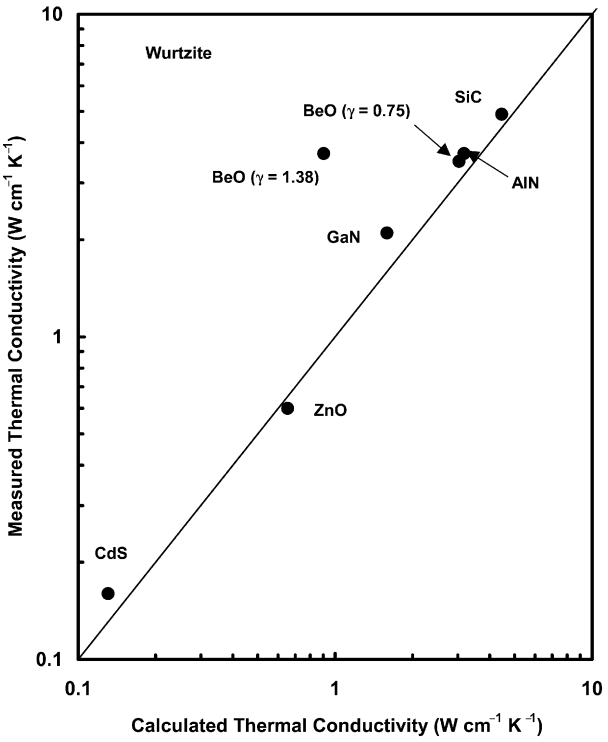

Fig. 2.5. Room-temperature thermal conductivity for the wurtzite compounds of Table 2.3 plotted against the thermal conductivity calculated from Eq. (2.13).

$n > 4$ that are potentially high-thermal-conductivity materials. One example is Si_3N_4. This compound assumes two crystal structures, known as the α and β phases, and is characterized by extreme hardness and toughness arising from predominantly covalent bonding [15]. Thus one might expect this compound to exhibit high thermal conductivity even though the crystal structure is not simple. Watari et al. [16] have reported the fabrication of hot-pressed, polycrystalline Si_3N_4 samples with thermal conductivity as high as $1.55\,\mathrm{Wcm^{-1}K^{-1}}$.

The α- and β-phases of Si_3N_4 are both hexagonal with $n = 28$ and $n = 14$, respectively [17]. Recently a third high-pressure phase, called γ-Si_3N_4, has been reported [18]. This phase crystallizes in the cubic spinel $MgAl_2O_4$ structure with $n = 14$. There are no thermal conductivity data on this structural modification in the literature. From recently published calculated phonon-dispersion curves [19] and thermal expansion data [20] one can estimate the average Debye temperature for these three structural modifications. Little information is available regarding the Grüneisen parameters of these compounds. He et al. [21] calculated $\gamma = 1.1$ for β-Si_3N_4. This value was derived from compressibility and bulk modulus data. Bruls et al. [22] report a high

temperature $\gamma = 0.63$ for β-Si_3N_4, not too different from the value $\gamma = 0.72$ reported by Slack and Huseby [23]. In order to obtain an upper limit for the calculated thermal conductivity we will assume the smaller value of γ for both the α- and β-phases. We will use the value $\gamma = 1.2$ determined for the γ-phase [20], noting that this value is consistent with $\gamma = 1.4$ for the isostructural compound $MgAl_2O_4$ [24].

The necessary parameters for all three Si_3N_4 phases are collected in Table 2.4, along with the calculated thermal conductivities. We have also included results for $MgAl_2O_4$ that serve to verify the validity of Eq. (2.13) for these more complex crystal structures. We see that the calculated thermal conductivity for the α- and β-phases both exceed $1\,\mathrm{Wcm^{-1}K^{-1}}$. The calculated value for β-Si_3N_4 suggests that even higher thermal conductivity than that measured by Watari et al. may be obtained in pure β-Si_3N_4 material. Reliable data on the Grüneisen parameters of these compounds would be very useful to verify the model for these compounds.

Ge_3N_4 also forms in the same α, β, and γ crystal structures [17, 25]. There are no experimental data on the thermal conductivity of these compounds; one would expect, however, in analogy to the Group IV semiconductors Si and Ge, that the heavier average mass of the germanium compounds will produce lower thermal conductivity than the silicon-based isostructures. From the available theoretical phonon-dispersion curves for the β-phase [26] and using the same value of γ as for β-Si_3N_4, we can make an estimate for the thermal conductivity of this compound; see Table 2.4.

Also very exciting from the point of view of high thermal conductivity are the predicted compounds C_3N_4 from the same α, β, and γ structural modifications [27, 28, 29] as well as a defective zincblende structure [30] and

Table 2.4. Calculated and experimental room-temperature thermal conductivity of several phases of Si_3N_4 and related compounds. n = number of atoms in the primitive unit cell; θ_a = Debye temperature of the acoustic phonon branch; γ = high-temperature Grüneisen constant; δ^3 = volume per atom; M = average atomic mass; κ_{calc} = calculated thermal conductivity from equation (2.13); κ_{exp} = measured thermal conductivity.

Compound	n	θ_a (K)	γ	δ (Å)	M (amu)	κ_{calc} ($\mathrm{Wcm^{-1}K^{-1}}$)	κ_{exp} ($\mathrm{Wcm^{-1}K^{-1}}$)
α-Si_3N_4	28	337	0.7	2.19	20.03	1.32	
β-Si_3N_4	14	485	0.7	2.18	20.03	2.61	1.55
γ-Si_3N_4	14	480	1.2	2.02	20.03	0.8	
γ-$MgAl_2O_4$	14	352	1.4	2.11	20.33	0.24	0.24
β-Ge_3N_4	14	243	0.63	2.31	39.11	0.65	
β-C_3N_4	14	∼650	0.7	1.91	13.15	3.5	
Be_2SiO_4	42	316	1.02	2.06	15.73	0.35	
Zn_2SiO_4	42	236	0.52	2.318	31.83	1.29	
Zn_2GeO_4	42	186	0.31	2.367	28.19	2.17	

even a CN phase [31]. Several of these compounds, originally proposed by Cohen [32], are predicted to have bulk moduli rivaling that of diamond. Of course, many of the features favoring high hardness, such as short bond lengths and strong covalent bond character, give rise to high thermal conductivity. Thus it is likely, given the results on Si_3N_4 and the smaller mass of the carbon atom, that at least some of the C-N phases, if they exist, may possess thermal conductivities at least as high as their Si-based counterparts. Since the predictions of their existence, there have been numerous attempts [33, 34, 35, 36, 37] to synthesize various structural modifications of C_3N_4 and related phases, though it is debatable whether any has been demonstrated unequivocally [38]. We can make a rough estimate of the thermal conductivity of these compounds, although we do not have the luxury of lattice dynamical calculations of the phonon dispersion and phonon density of states. Rather, we make an estimate of the high-temperature Debye temperature from the theoretical bulk and shear moduli [39] using the method of Ravindran et al. [40]. The results are shown in Table 2.4. The predicted thermal conductivity of β-C_3N_4 exceeds that of β-Si_3N_4; if reasonably large crystals of the carbon nitrides become available it would be very interesting to study their thermal conductivity.

Be_2SiO_4 (phenacite) and Zn_2SiO_4 (willemite) also possess the β-Si_3N_4 structural modification but with two of the silicon atoms replaced by Be and Zn, respectively [41]. As with silicon nitride itself, these and other phenacites are typified by Grüneisen parameters on the order of or, in some cases, much less than, unity. Thus they could be potentially high-thermal-conductivity materials even though they have fairly large $n = 42$. From thermal expansion data the high-temperature limits of θ and γ have been determined [23] and θ_a calculated from Eq. (2.12). The estimated room-temperature thermal conductivity of these and related compounds are displayed in Table 2.5. Zn_2SiO_4 and Zn_2GeO_4 both display calculated thermal conductivity in excess of $1\,\mathrm{Wcm^{-1}K^{-1}}$; the case of Zn_2GeO_4, is very interesting because this compound has both a large n and large M. Again we see high thermal conductivity arising from a very small Grüneisen parameter; this suggests that looking for compounds with similarly low γ is another route for discovering high-thermal-conductivity materials. The tendency for a crystal to possess a low γ may be related to the openness of the structure [23]. This openness

Table 2.5. Calculated and experimental room-temperature thermal conductivity of some boron-containing compounds. Parameters are defined in Table 2.4.

Compound	n	θ_a (K)	γ	δ (Å)	M (amu)	κ_{calc} ($\mathrm{Wcm^{-1}K^{-1}}$)	κ_{exp} ($\mathrm{Wcm^{-1}K^{-1}}$)
$B_{12}As_2$	14	390	0.75	2.10	19.97	1.10	1.2
$B_{12}P_2$	14	481	0.75	2.06	13.69	1.38	0.38
$B_{12}O_2$	14	520	0.75	2.05	11.55	1.47	

allows more freedom of movement for the transverse phonon modes, and it is these modes that generally possess lower Grüneisen parameters [13]. Further detailed experimental and theoretical studies on the Grüneisen parameters and thermal conductivity of the phenacites and related structures would be very desirable to determine whether these compounds in fact possess small γ and large κ.

2.3.4 Icosahedral Boron Compounds

The element boron occurs in an α-structure, consisting of B_{12} icosahedra linked together with covalent bonds, and a β-structure consisting of B_{84} units [42]. Several boron-rich compounds also form as variations of the icosahedral B_{12} units [43]. From the point of view of high thermal conductivity, some of the most interesting of these are the compounds $B_{12}As_2$, $B_{12}P_2$, and $B_{12}O_2$. These compounds all have $n = 14$. The last of these, sometimes referred to as boron suboxide, was recently reported [44] to have a hardness exceeding that of cubic BN. Slack et al. [45] measured the thermal conductivity of a single crystal of $B_{12}As_2$ and an impure oligocrystalline $B_{12}P_2$ sample. Table 2.5 presents the necessary parameters to calculate the thermal conductivity. For $B_{12}As_2$ and $B_{12}P_2$, θ_a was calculated using Eq. (2.12) from θ-values estimated from the specific heat and elastic constants of similar boron compounds [45, 46, 47]; their γ-values were taken equal to that of β-boron [1]. We see that the model reproduces quite well the thermal conductivity of $B_{12}As_2$. As mentioned by Slack et al., the $B_{12}P_2$ they measured was neither a single crystal nor a very pure specimen, and examination of the temperature dependence of the thermal conductivity would suggest that its thermal conductivity at room temperature is partially limited by extrinsic scattering processes. It is likely that pure crystals of $B_{12}P_2$ and boron suboxide will have room-temperature thermal conductivity exceeding $1\,\mathrm{Wcm^{-1}K^{-1}}$.

In addition to these compounds, there are many other structures in the B-C-N triangle that exhibit hard or superhard behavior [48, 49], and it is possible that at least some of these may be high-thermal-conductivity materials. This is a rich field that currently is largely unexplored from the point of view of thermal transport and is deserving of further experimental and theoretical scrutiny.

2.3.5 Graphite and Related Materials

The form of carbon known as graphite is a hexagonal structure, $n = 4$, consisting of carbon atoms linked together in hexagons [50]. The C-C distance within the planes is 1.42 Å, nearly the same as that in benzene; the interplanar distance, on the other hand, is 3.40 Å. These differences reflect the very different nature of the bonding within a plane and between planes in graphite, with the former essentially a covalent sp^2-bonding arrangement and

the latter a weak Van der Waals type of bonding. The thermal conductivity of graphite has been extremely well studied both experimentally and theoretically; for a more complete discussion the reader is referred to the review [51] and monograph [52] by Kelly, which include discussions of the influence of defects and various types of quasi-crystalline forms of this material. Here we only briefly consider graphite in its most perfect form, namely single crystals or highly oriented polycrystalline pyrolytic graphite.

Up to now, we have largely ignored the effects of anisotropy because for the crystals we have considered these effects are either absent or quite small. In graphite, however, the highly anisotropic nature of bonding manifests itself as an enormous anisotropy in the conduction of heat. Because of the crystal symmetry there are only two principle conductivities: that in the plane and that perpendicular to the plane, or along the so-called c-axis. Figure 2.6 shows composite curves of in-plane and c-axis thermal conductivity of graphite; these represent an average of many measurements that have been done over the last half century [53, 54, 55, 56, 57].

In the context of the simple model we have considered in this review, the anisotropy is due to the large difference in Debye temperature for phonon transport in the plane versus along the c-axis. These Debye temperatures can be estimated from a fit to the specific heat assuming a combination of "in-plane" and "out-of-plane" vibrations [58] and applying Eq. (2.12) to determine the Debye temperature of the acoustic modes.

Because of the strong intraplanar covalent bonding, we will assume for in-plane transport a Grüneisen parameter similar to that of diamond, while for out-of-plane transport we take $\gamma = 2$. The calculated thermal conductivity from Eq. (2.13) is shown in Table 2.6, and again we see that the simple model can account reasonably well for the magnitude of κ both perpendicular and parallel to the basal plane in graphite. A more complete theory of the thermal conductivity of graphite is based on the lattice dynamics models of in-plane and out-of-plane phonon modes (Komatsu [58]; Krumhansl and Brooks [61]) and the contribution of each of these to the basal plane and c-axis thermal conductivities. Extrinsic scattering mechanisms may also play an important role. The reader is referred to the book by Kelly [51] for further details.

Table 2.6. Thermal conductivity of graphite and BN in the basal plane (xy) and perpendicular to the c-axis (z).

Compound	n	θ_a (K)	γ	δ (Å)	M (amu)	κ_{calc} ($\text{Wcm}^{-1}\text{K}^{-1}$)	κ_{exp} ($\text{Wcm}^{-1}\text{K}^{-1}$)
Graphite-xy	4	1562	0.75	2.05	12.01	27	10–20
Graphite-z	4	818	2	2.05	12.01	0.5	0.06
BN-xy	4	1442	0.75	2.05	12.40	22	2–3
BN-z	4	755	2	2.05	12.4	0.4	∼0.02

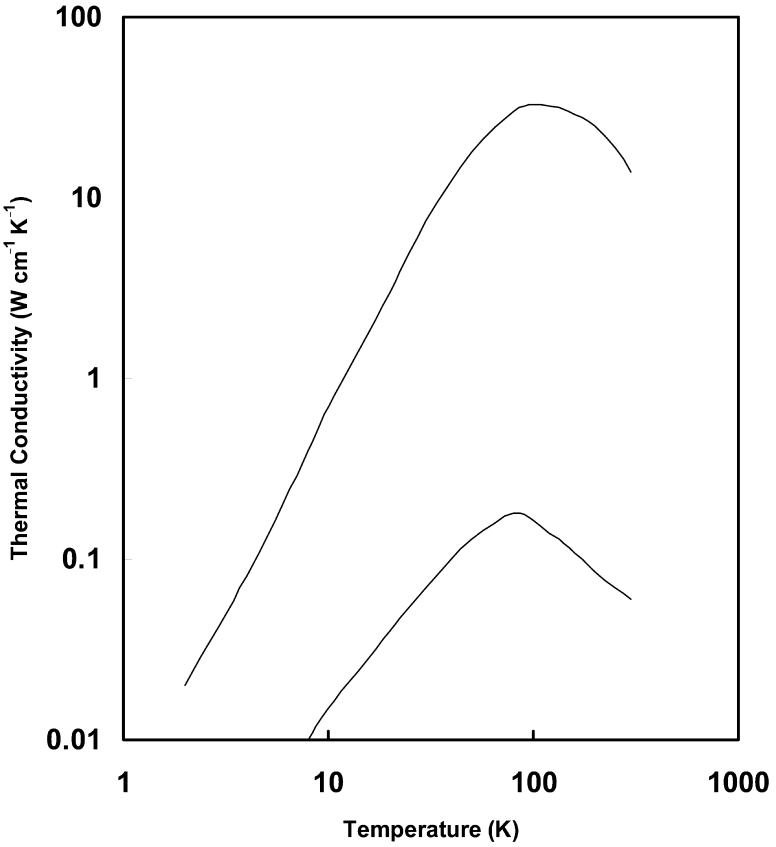

Fig. 2.6. Thermal conductivity of highly oriented graphite parallel (upper curve) and perpendicular (lower curve) to the basal plane.

Analogous to graphite, there exists a hexagonal form of boron nitride [62]. Measurements of the thermal conductivity have been made on sintered compacts with crystallite sizes on the order of 1000 Å or less [63]. We see (Table 2.7) again a reasonable agreement with the model using parameters derived in a similar fashion to those of graphite. Again, as in the case of graphite, a more complete theory of thermal conductivity in this hexagonal structural modification would take into account the details of the lattice dynamics of this structure.

Recently, many other forms of carbon, including fibers, sheets, C60, graphene sheets, and nanotubes, have been demonstrated or predicted. Some of these have or are expected to have high thermal conductivity. Chapter 8 of this volume is devoted to the thermal conductivity of carbon nanotubes and the reader is referred to it for further information.

2.4 Thermal Conductivity of Wide-Band-Gap Semiconductors: Silicon Carbide, Aluminum Nitride, and Gallium Nitride

We have seen that among the select group of materials with high thermal conductivity are the Group IV and Group III–V wide-band-gap semiconductors SiC, AlN, and GaN. Because of their wide gap, high-saturation electron velocities, and high thermal conductivity, these and related compounds have undergone significant development over the last decade for optoelectronic, high-frequency, high-temperature, and high-power device applications [64]. There has thus been an increase in availability of high-quality single crystals. Because of the importance of the thermal conductivity for many of these applications, we will look at these compounds in a little more detail in this section. Our emphasis is on the thermal conductivity of nearly defect-free single crystals and the influence of low levels of defects and impurities; Chapters 5 and 6 address the interesting and important subject of polycrystalline ceramics of SiC and AlN.

SiC was the earliest of this trio to undergo development as a substrate and active material for electronics applications. Much earlier, however, Slack [65] presented the first, and for many years the only, detailed characterization of the thermal conductivity of SiC single crystals and provided the first identification of this compound as a high-thermal-conductivity material. Slack noted that electrically active impurities had a noticeably stronger effect on the thermal conductivity than neutral impurities. Burgemeister et al. [66] studied several n- and p-type single crystals in the region around room temperature and showed that the thermal conductivity displayed a strong dependence on carrier concentration. Morelli et al. [67] studied several single crystals of different electron concentrations as a function of temperature. These results showed that samples with higher electron concentrations not only had lower thermal conductivity, but assumed a quadratic, as opposed to a T^3, temperature dependence at low temperature, an effect they ascribed to scattering of phonons by electrons in an impurity band. Müller et al. [68] measured the thermal conductivity of a single crystal from room temperature up to 2300 K. Some of these data are summarized in Fig. 2.7.

The data on SiC afford an example of how the relaxation-time approximation and the Debye model may be used to understand the magnitude and temperature dependence of the thermal conductivity. Theoretical fits of the lattice thermal conductivity may be performed using the standard expression (2.6). The phonon-scattering relaxation rate τ_C^{-1} can be written as:

$$\tau_C^{-1} = \frac{v}{L} + A\omega^4 + B\omega^2 T \exp\left(-\frac{\theta_D}{3T}\right) \tag{2.14}$$

where the first term on the right-hand side represents scattering of the crystal boundaries with an effective crystal diameter L; the second term describes any

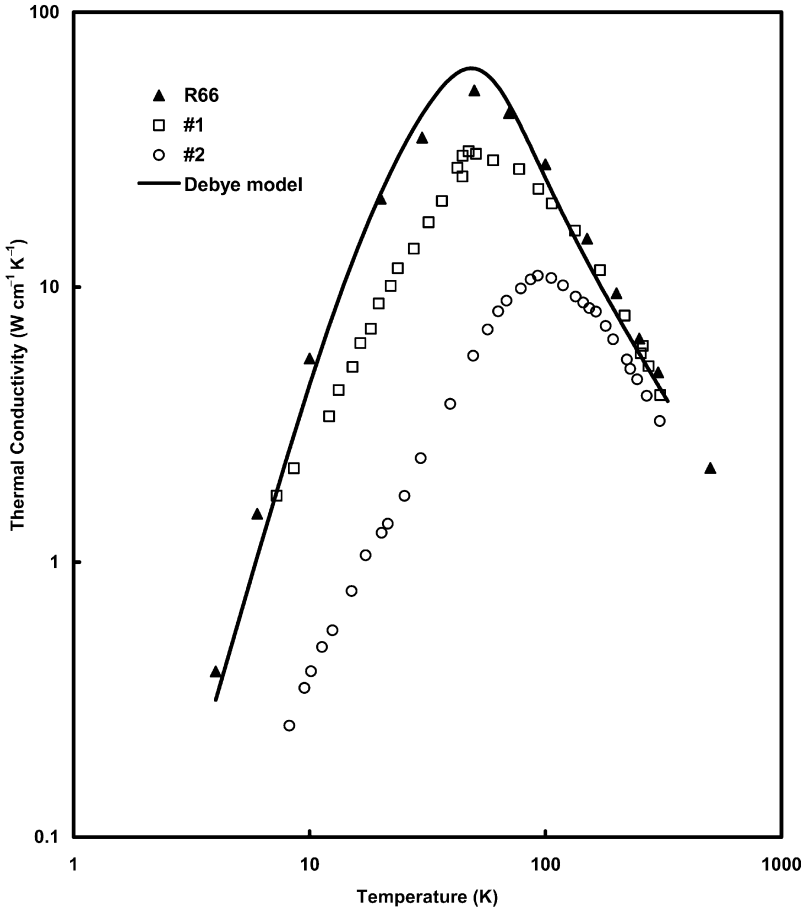

Fig. 2.7. Thermal conductivity of various single crystals of SiC. R66: pure crystal Slack [65]; #1 and #2: crystals [67] with electron concentrations of 3.5×10^{16} and $2.9 \times 10^{18}\,\mathrm{cm}^{-3}$, respectively.

point-defect scattering that may be present in the crystal; and the third term represents intrinsic phonon-phonon Umklapp scattering. The data in Fig. 2.7 for the purest sample of SiC can be fit with this expression using a Debye temperature of $\theta_D = 800\,\mathrm{K}$.

The question of the influence of the electrical state of the sample on the thermal conductivity is important for the development of semi-insulating substrates for high-power electronic devices. Currently three-inch-diameter SiC substrates are commercially available and four-inch substrates have been demonstrated in the laboratory. Semi-insulating substrates are fabricated either by introducing vanadium during the growth process [69], thereby providing a deep level that traps free carriers, or by reducing as much as possible the presence of nitrogen during growth while providing "native" defects that

can trap any remaining carriers [70]. In either case, to the extent that free carriers are eliminated, any reduction in the thermal conductivity below the "intrinsic" conductivity will be due to the presence of the trapping species. Studies of the thermal conductivity of silicon carbide containing these deep-level impurities would be very revealing in this regard.

Though not nearly as intense as the development of SiC substrates, GaN substrate development has accelerated dramatically over the last few years. As of this writing, two-inch wafers have been demonstrated and are becoming commercially available. Until recently, the only thermal-conductivity data available were those of Sichel and Pankove [71]. More recently, Pollak and coworkers have studied the local thermal conductivity of epitaxial layers of GaN using a scanning thermal microscopy technique. They found that the thermal conductivity of these layers depends strongly on the dislocation density, ranging from values as low as $1.3\,\mathrm{Wcm^{-1}K^{-1}}$ for high-dislocation density films to greater than $2\,\mathrm{Wcm^{-1}K^{-1}}$ for regions on films containing two orders of magnitude fewer dislocations [72]. Further studies by Pollak's group on n-type GaN layers showed [73] that the thermal conductivity also decreased strongly with increasing electronic concentration in the range 10^{17}–$10^{19}\,\mathrm{cm^{-3}}$. Slack et al. [74] recently reported the temperature-dependent thermal conductivity on a high-quality single crystal of GaN; these results are shown in Fig. 2.8 along with the earlier results of Sichel and Pankove. This single crystal had a room-temperature thermal conductivity of $2.1\,\mathrm{Wcm^{-1}K^{-1}}$ and the temperature dependence could be fit with Eq. (2.6) using a Debye temperature of approximately 525 K. The large difference in the conductivities between this sample and that of Sichel and Pankove was attributed to the presence of oxygen in the latter sample.

The suggestion by Slack et al. that the difference in conductivities of these two GaN samples is due to the presence of oxygen was based on the well-documented studies of the thermal conductivity of the isostructural compound AlN. Although substrate development for this wide-band-gap semiconductor is still in its nascent stage [75], some information on the thermal conductivity is available in the literature. Slack et al. [76] studied several single crystals and found large differences in thermal conductivity that seemed to depend on oxygen content. A sample that was nearly free of impurities and defects had a room-temperature thermal conductivity of $3.5\,\mathrm{Wcm^{-1}K^{-1}}$, while those containing measurable quantities of oxygen impurity had a lower conductivity characterized by a depression or dip in the curve as a function of temperature. Some of these results, along with more recent results of Slack et al [74] on a sample containing about 1000 ppm oxygen, are shown in Fig. 2.9.

In order to gain a deeper understanding of the influence of oxygen on the thermal conductivity of AlN, it is useful to understand the kinetics of oxygen impurities in this compound. Oxygen in the aluminum nitride lattice has its origin in small amounts of Al_2O_3 dissolved in the AlN grains. At high

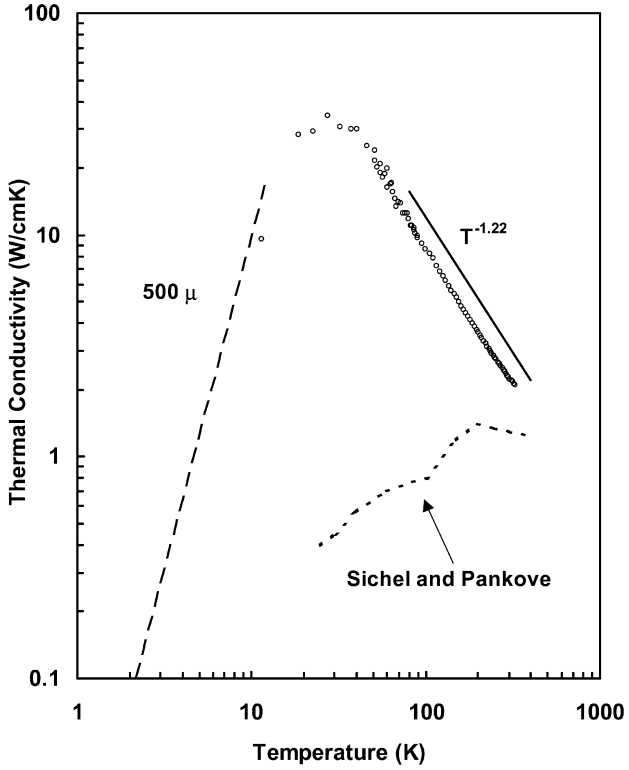

Fig. 2.8. Thermal conductivity of GaN as a function of temperature. Open points: data of Slack et al. [74]; lower dotted line: results of Sichel and Pankove [71]. Dashed line shows low-temperature boundary limit, assuming a crystal dimension of 500 microns.

temperatures, dissolution of Al_2O_3 occurs according to the reaction:

$$Al_2O_3 \longrightarrow 2Al + 3O_N + V_{Al}, \tag{2.15}$$

where the subscripts N and Al, respectively, indicate that the O atoms occupy the nitrogen site and the vacancy occurs on the aluminum site. Thus, the presence of oxygen in the AlN lattice is always accompanied by the presence of vacancies, with the oxygen-vacancy ratio of 3:1. This is because the Al/O ratio in Al_2O_3 is 2:3 and the Al/N ratio in aluminum nitride is 1:1. The presence of an impurity (in this case oxygen) or a defect (in this case the vacancy) in an otherwise perfect aluminum nitride lattice will cause a reduction in thermal conductivity. This reduction has been well studied [2] and arises due to differences in the mass and size of the impurity or defect. These differences cause a scattering of the heat-carrying lattice vibrations; the scattering rate for this process is proportional to the square of the difference in mass between the host atom and the impurity. The mass difference between oxygen and nitrogen

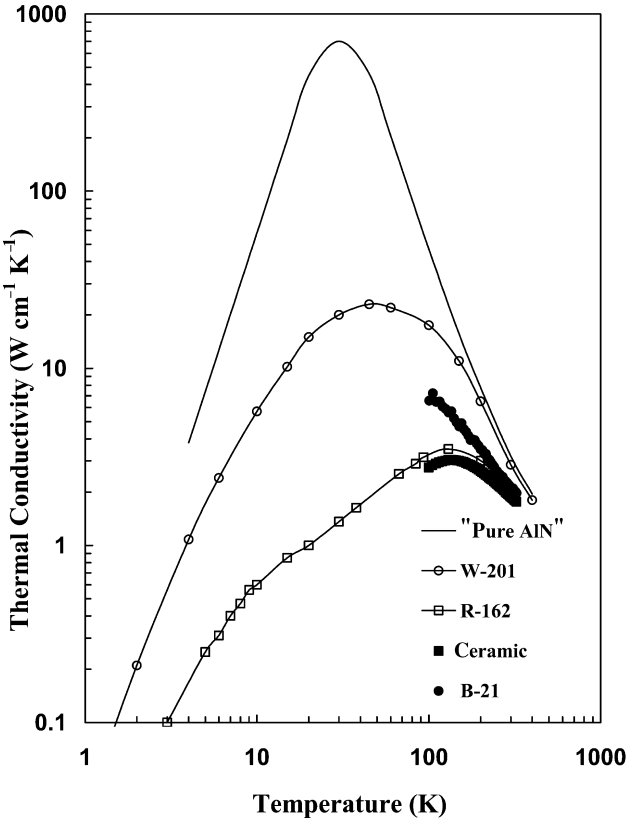

Fig. 2.9. Thermal conductivity of single-crystal AlN. "Pure AlN" is the calculated result for a crystal containing no impurities; samples W-201, R-162, and B-21 are single crystals with varying amounts of oxygen concentrations; see text. A ceramic sample is shown for comparison.

is not large; thus, the direct effect of oxygen on the thermal conductivity of the aluminum nitride is small. On the other hand, the fractional mass difference between a vacancy and aluminum is 100 percent, and this gives rise to a very large scattering rate. Thus, the lowering of the thermal conductivity by oxygen in AlN is really due to the presence of the vacancy on the aluminum site, which inexorably accompanies the less malevolent oxygen. The influence of oxygen is well described by the additive resistivity approximation [76]:

$$W_{\text{total}} = W_{\text{pure}} + \Delta W_1 \tag{2.16}$$

were W_{total} is the measured thermal resistivity ($=1/\kappa_{\text{total}}$), W_{pure} is the thermal resistivity of a pure AlN crystal ($W_{\text{pure}} = 0.3\,\text{K cm W}^{-1}$), and ΔW is the increase in resistivity due to the presence of oxygen and is proportional to the oxygen concentration. For an oxygen concentration α by weight, the

data of Fig. 2.3 yield $\Delta W = 110\alpha$ at room temperature. Thus, to obtain high thermal conductivity ($>0.5\,\mathrm{Wcm^{-1}K^{-1}}$), the oxygen concentration in AlN must be below about 1.5 percent. The influence of oxygen on the thermal conductivity of AlN is particularly important for the commercial manufacture of ceramic polycrystalline substrates of this material, as these ceramics are sintered using an oxide binder [77]. The thermal conductivity of AlN ceramics is discussed in detail in Chapter 5.

2.5 Isotope Effect in High Lattice Thermal Conductivity Materials

Since the early work of Pomeranchuk [78], it has been known that isotopes, due to their mass difference, can scatter phonons and decrease thermal conductivity. This effect was discussed also by Slack [79]. Geballe and Hull [80] provided unequivocal evidence for the influence of isotopes on the thermal conductivity with their experiments on natural abundance and isotopically purified germanium.

With the ready availability of isotopically purified source materials, the isotope effect has undergone reexamination over the last decade. Isotopically purified diamond [81, 82, 83, 84] displays a room-temperature isotope effect on the order of 40 percent. More recently, Asen-Palmer et al. [59] carried out a very thorough investigation of the isotope effect in germanium and showed that an isotopically purified sample had a 30 percent larger κ than natural abundance Ge. Very recently, Ruf et al. [85] reported an isotope effect in silicon of 60 percent at 300 K, although the same authors [86] subsequently downgraded the magnitude to 10 percent.

The magnitude of the isotope effect in these materials is at first surprising because a simple estimate using the standard Debye theory of lattice thermal conductivity [3] (Eq. 2.6) yields increases in all cases of 5 percent or less. A more thorough and complete understanding of the isotope effect in these materials must recognize the importance of normal phonon-phonon scattering processes [87, 88, 89] within the context of the Callaway model. In the case of diamond it has been argued [87, 88, 89] that including the effect of normal phonon-scattering processes can explain the experimental result, although assuming infinitely rapid normal processes can only qualitatively fit the data [82].

Recently an extension of the Callaway model was provided by Asen-Palmer et al. [59], who successfully modeled the lattice thermal conductivity of Ge by not only using the Callaway formalism but also by considering the explicit mode dependence of the thermal conductivity and summing over one longitudinal (κ_L) and two degenerate transverse (κ_T) phonon branches:

$$\kappa = \kappa_L + 2\kappa_T, \tag{2.17}$$

where

$$\kappa_L = \kappa_{L1} + \kappa_{L2}. \tag{2.18}$$

The partial conductivities κ_{L1} and κ_{L2} are the usual Debye-Callaway terms given by:

$$\kappa_{L1} = \frac{1}{3} C_L T^3 \int_0^{\theta_L/T} \frac{\tau_C^L(x) x^4 e^x}{(e^x - 1)^2} dx, \tag{2.19}$$

$$\kappa_{L2} = \frac{1}{3} C_L T^3 \frac{\left[\int_0^{\theta_L/T} \frac{\tau_C^L(x) x^4 e^x}{\tau_N(x)(e^x - 1)^2} dx \right]^2}{\int_0^{\theta_L/T} \frac{\tau_C^L(x) x^4 e^x}{\tau_N^L(x) \tau_R^L(x)(e^x - 1)^2} dx}, \tag{2.20}$$

and similarly, for the transverse phonons,

$$\kappa_{T1} = \frac{1}{3} C_T T^3 \int_0^{\theta_T/T} \frac{\tau_C^T(x) x^4 e^x}{(e^x - 1)^2} dx, \tag{2.21}$$

$$\kappa_{T2} = \frac{1}{3} C_T T^3 \frac{\left[\int_0^{\theta_T/T} \frac{\tau_C^T(x) x^4 e^x}{\tau_N^T(x)(e^x - 1)^2} dx \right]^2}{\int_0^{\theta_T/T} \frac{\tau_C^T(x) x^4 e^x}{\tau_N^T(x) \tau_R^T(x)(e^x - 1)^2} dx}. \tag{2.22}$$

In these expressions, $(\tau_N)^{-1}$ is the scattering rate for normal phonon processes; $(\tau_R)^{-1}$ is the sum of all resistive scattering processes; and $(\tau_C)^{-1} = (\tau_N)^{-1} + (\tau_R)^{-1}$, with superscripts L and T denoting longitudinal and transverse phonons, respectively. The quantities θ_L and θ_T are Debye temperatures appropriate for the longitudinal and transverse phonon branches, respectively, and

$$C_{L(T)} = \frac{k_B^4}{2\pi^2 \hbar^3 v_{L(T)}} \tag{2.23}$$

and

$$x = \frac{\hbar \omega}{k_B T}. \tag{2.24}$$

Here ω is the phonon frequency and $v_{L(T)}$ are the longitudinal (transverse) acoustic phonon velocities, respectively.

The temperature dependence and the magnitude of the lattice thermal conductivity are determined by the temperature and frequency dependence of the scattering rates comprising $(\tau_N)^{-1}$ and $(\tau_R)^{-1}$, their coefficients, and the Debye temperatures and phonon velocities. The resistive scattering rate includes contributions from Umklapp processes, isotope scattering, and

Table 2.7. Percentage Increase in Room-Temperature Thermal Conductivity due to the Isotope Effect in Some Group IV and Group III–V semiconductors.

Element/ Compound	$\Delta\kappa/\kappa^{*}$ (%)	$\Delta\kappa/\kappa^{**}$ (%)	$\Delta\kappa/\kappa^{***}$ (%)
Ge	30	28	30
Si		12	60
C		23	35–45
SiC		36	
GaN		5	
BN		125	

* Model [59].
** Model [60].
*** Experimental results.

boundary scattering. Using the isotope scattering rate of Klemens [90] and appropriately adjusting the coefficients of the normal and Umklapp phonon-scattering rates, Asen-Palmer et al. [59] were able to quantitatively fit their experimental results over the entire temperature range of 10–300 K.

Recently, Morelli et al. [60] extended and modified this approach to model the isotope effect in diamond, silicon, germanium, silicon carbide, gallium nitride, and boron nitride. As mentioned previously, experimental data exist for the cases of diamond, silicon, and germanium. The model was able to account for the magnitude of the isotope effect all these semiconductors. Table 2.7 displays the measured and predicted isotope effect in these Group IV and Group III–V semiconductors at room temperature. Particularly noteworthy is the predicted magnitude of the isotope effect in boron nitride. This has its origin in the light atom masses and the natural abundance distribution of boron isotopes. Although boron nitride single crystals are extremely difficult to fabricate, it would be very desirable to study the isotope effect in this wide-band-gap semiconductor.

2.6 Summary

The intrinsic lattice thermal conductivity of crystalline solids near the Debye temperature can be understood on the basis of a simple model based on information that can be obtained from the crystal structure and lattice dynamics or phonon dispersion. The measured thermal conductivity of simple crystal structures such as rocksalt, zincblende, diamond, and wurtzite agree quite well with the predictions of the model. The model can be extended to other crystal structures to predict the thermal conductivity of new materials.

Several materials have been discussed that can be categorized as having high thermal conductivity. These include most of the simple zincblende, diamond, and wurtzite structure compounds. Various compounds possessing the hexagonal Si_3N_4 structure have been found or are predicted on the basis of this model to have high thermal conductivity, as have several compounds based on icosahedral boron structures. High lattice thermal conductivity compounds may be discovered in structures within the B-C-N or B-Si-N triangles and in similar triangles with oxygen substituted for nitrogen. This predicted high thermal conductivity would arise due to the strong covalent bonding and potentially low Grüneisen parameters of these structural modifications. The isotope effect may be used to increase the thermal conductivity of several wide-band-gap semiconductors, especially those containing boron.

Acknowledgments

The authors would like to acknowledge Dr. Joseph Heremans for useful discussions and a critical reading of the manuscript.

References

[1] G. A. Slack, *Solid St. Phys.* **34**, 1 (1979); G. A. Slack, *J. Phys. Chem. Solids* **34**, 321 (1973).
[2] P. G. Klemens, *Solid St. Phys.* **7**, 1 (1958).
[3] R. Berman, *Thermal Conduction in Solids* (Clarendon Press, Oxford, 1976).
[4] K. Watari and S. L. Shinde, Eds. *Mat. Res. Soc. Bull.* **26**, 440 (2001).
[5] S. Pettersson, *J. Phys. C: Solid St. Phys.* **20**, 1047 (1987).
[6] C. Domb and L. Salter, *Phil. Mag.* **43**, 1083 (1952).
[7] J. Callaway, *Phys. Rev.* **113**, 1046 (1959).
[8] G. Leibfried and E. Schlömann, *Nachr. Akad. Wiss. Göttingen II* **a(4)**, 71 (1954).
[9] C. L. Julian, *Phys. Rev.* **137**, A128 (1965).
[10] O. L. Anderson, *J. Phys. Chem. Solids* **12**, 41 (1959).
[11] C. H. Xu, C. Z. Wang, C. T. Chan, and K. M. Ho, *Phys. Rev. B* **43**, 5024 (1991).
[12] P. Pavone, K. Karch, O. Schütt, W. Windl, D. Strauch, P. Giannozzi, and S. Baroni, *Phys. Rev. B* **48**, 3156 (1993).
[13] G. Kern, G. Dresse, and J. Hafner, *Phys. Rev. B* **59**, 8551 (1999).
[14] Calculated from the data of G. A. Slack and S. F. Bartram, *J. Appl. Phys.* **46**, 89 (1975) and C. F. Cline, J. L. Dunegan, and G. W. Henderson, *J. Appl. Phys.* **38**, 1944 (1967).
[15] R. N. Katz, *Science* **84**, 208 (1980).
[16] K. Watari, K. Hirao, M. E. Brito, M. Toriyama, and S. Kanzaki, *J. Mater. Res.* **14**, 1538 (1999).
[17] R. W. G. Wyckoff, *Crystal Structures* (Interscience, New York, 1948), Vol. 2, p. 157.

[18] A. Zerr, G. Miehe, G. Serghio, M. Schwarz, E. Kroke, R. Riedel, H. Fue, P. Kroll, and R. Boehler, *Nature* **400**, 340 (1999).
[19] W.-Y. Ching, Y.-N. Xu, J. D. Gale, and M. Rühle, *J. Am. Cer. Soc.* **81**, 3189 (1998).
[20] J. Z. Jiang, H. Lindelov, L. Gerward, K. Stahl, J. M. Recio, P. Mori-Sanchez, S. Carlson, M. Mezouar, E. Dooryhee, A. Fitch, and D. J. Frost, *Phys. Rev. B* **65**, 161202 (2002).
[21] H. He, T. Sekine, T. Kobayashi, and H. Hirosaki, *Phys. Rev. B* **62**, 11412 (2000).
[22] R. J. Bruls, H. T. Hintzen, G. de With, R. Metselaar, and J. C. van Miltenburg, *J. Phys. Chem. Sol.* **62**, 783 (2001).
[23] G. A. Slack and I. C. Huseby, *J. Appl. Phys.* **53**, 6817 (1982).
[24] Z. P. Chang and G. R. Barsch, *J. Geophys. Res.* **78**, 2418 (1973).
[25] G. Serghiou, G. Miehe, O. Tschauner, A. Zerr, and R. Boehler, *J. Chem. Phys.* **111**, 4659 (1999).
[26] J. Dong, O. F. Sankey, S. K. Deb, G. Wolf, and P. F. McMillan, *Phys. Rev. B* **61**, 11979 (2000).
[27] D. Teter and R. J. Hemley, *Science* **271**, 53 (1996).
[28] A. Y. Liu and R. M. Wentzcovitch, *Phys. Rev. B* **50**, 10362 (1994).
[29] A. Y. Liu and M. L. Cohen, *Science* **245**, 841 (1989).
[30] J. Martin-Gil, F. J. Martin-Gil, M. Sarikayta, M. Qian, M. José-Yacamán, A. Rubio, *J. Appl. Phys.* **81**, 2555 (1997).
[31] M. Côté and M. L. Cohen, *Phys. Rev. B* **55**, 5684 (1997).
[32] M. L. Cohen, *Phys. Rev. B* **32**, 7988 (1985).
[33] C. Niu, Y. Z. Lu, and C. M. Lieber, *Science* **261**, 334 (1993).
[34] K. M. Liu, M. L. Cohen, E. E. Haller, W. L. Hansen, A. Y. Liu, and I. C. Wu, *Phys. Rev. B* **49**, 5034 (1994).
[35] H. W. Song, F. Z. Cui, X. M. He, W. Z. Li, and H. D. Li, *J. Phys. Cond. Matter* **6**, 6125 (1994).
[36] T.-Y. Yen and C.-P. Chou, *Solid St. Comm.* **95**, 281 (1995).
[37] Y. Chen, L. Guo, and E. Wang, *Phil. Mag. Lett.* **75**, 155 (1997).
[38] P. Ball, *Nature* **403**, 871 (2000).
[39] www.dirac.ms.virginia.edu/∼emb3t/eos/html/final.html
[40] P. Ravindran, L. Fast, P. A. Korzhavyi, B. Johansson, J. Wills, and O. Eriksson, *J. Appl. Phys.* **84**, 4891 (1998).
[41] R. W. G. Wyckoff, *Crystal Structures* (Interscience, New York, 1948), Vol. 3, p. 133.
[42] R. W. G. Wyckoff, *Crystal Structures* (Interscience, New York, 1948), Vol. 1, p. 19.
[43] J. L. Hoard and R. E. Hughes, in *The Chemistry of Boron and Its Compounds*, ed. E. L. Muetterties (Wiley, New York, 1967), Chapter II.
[44] D. He, Y. Zhao, L. Daemen, J. Qian, T. D. Shen, and T. W. Zerda, *Appl. Phys. Lett.* **81**, 643 (2002).
[45] G. A. Slack, D. W. Oliver, and F. H. Horn, *Phys. Rev. B* **4**, 1714 (1971).
[46] G. A. Slack, *Phys. Rev.* **139**, A507 (1965).
[47] E. F. Steigmeier, *Appl. Phys. Lett.* **3**, 6 (1963).
[48] S. Vepřek, *J. Vac. Sci. Technol.* **17**, 2401 (1999).
[49] P. Rogl and J. C. Schuster, eds., *Phase Diagrams of Ternary Boron Nitride and Silicon Nitride Systems* (ASM International, Metals Park, OH, 1992).

[50] R. W. G. Wyckoff, *Crystal Structures* (Interscience, New York, 1948), Vol. 1, p. 27.
[51] B. T. Kelly, in *Chemistry and Physics of Carbon*, ed. P. L. Walker, Jr. (Marcel Dekker, New York, 1969), Vol. 5, p. 119.
[52] B. T. Kelly, *Physics of Graphite* (Applied Science Publishers, London, 1981).
[53] G. A. Slack, *Phys. Rev.* **127**, 694 (1962).
[54] C. A. Klein and M. G. Holland, *Phys. Rev.* 136, A575 (1964).
[55] M. G. Holland, C. A. Klein, and W. B. Straub, *J. Phys. Chem. Solids* **27**, 903 (1966).
[56] A. de Combarieu, *J. Phys. (France)* **28**, 931 (1968).
[57] D. T. Morelli and C. Uher, *Phys. Rev. B* **31**, 6721 (1985).
[58] K. Komatsu, *J. Phys. Soc. Japan* **10**, 346 (1955).
[59] M. Asen-Palmer, K. Bartkowski, E. Gmelin, M. Cardona, A. P. Zhernov, A. V. Inyushkin, A. Taldenkov, V. I. Ozhogin, K. M. Itoh, and E. E. Haller, *Phys. Rev. B* **56**, 9431 (1997).
[60] D. T. Morelli, J. P. Heremans, and G. A. Slack, *Phys. Rev. B* **66**, 195304 (2002).
[61] J. A. Krumhansl and H. Brooks, *J. Chem. Phys.* **21**, 1663 (1953).
[62] R. W. G. Wyckoff, *Crystal Structures* (Interscience, New York, 1948), Vol. 1, p. 184.
[63] A. Simpson and A. D. Stuckes, *J. Phys. C* **4**, 1710 (1971).
[64] H. Morkoç, *Nitride Semiconductors and Devices* (Springer Verlag, New York, 1999).
[65] G. A. Slack, *J. Appl. Phys.* **35**, 3460 (1964).
[66] E. A. Burgemeister, W. von Muench, and E. Pettenpaul, *J. Appl. Phys.* **50**, 5790 (1979).
[67] D. T. Morelli, J. P. Heremans, C. P. Beetz, W. S. Yoo, and H. Matsunami, *Appl. Phys. Lett.* **63**, 3143 (1993).
[68] St. G. Müller, R. Eckstein, J. Fricke, D. Hofmann, R. Hofmann, R. Horn, H. Mehling, and O. Nilsson, *Materials Science Forum* **264–8**, 623 (1998).
[69] H. McD. Hobgood, R. C. Glass, G. Augustine, R. H. Hopkins, J. Jenny, M. Skowronski, W. C. Mitchel, and M. Roth, *Appl. Phys. Lett.* **66**, 1364 (1995).
[70] C. H. Carter, Jr., M. Brady, and V. F. Tsvetkov, *US Patent Number 6,218,680* (April 17, 2001).
[71] E. K. Sichel and J. I. Pankove, *J. Phys. Chem. Solids* **38**, 330 (1977).
[72] D. I. Florescu, V. M. Asnin, F. H. Pollak, A. M. Jones, J. C. Ramer, M. J. Schurman, and I. Ferguson, *Appl. Phys. Lett.* **77**, 1464 (2000); D. Kotchetkov, J. Zou, A. A. Balandin, D. I. Florescu, and F. H. Pollak, *Appl. Phys. Lett.* **79**, 4316 (2001).
[73] D. I. Florescu, V. M. Asnin, F. H. Pollak, R. J. Molnar, and C. E. C. Wood, *J. Appl. Phys.* **88**, 3295 (2000).
[74] G. A. Slack, L. J. Schowalter, D. T. Morelli, and J. A. Freitas, Jr., *Proc. 2002 Bulk Nitride Workshop*, Amazonas, Brazil (to appear in *Journal of Crystal Growth*).
[75] www.crystal-is.com
[76] G. A. Slack, R. A. Tanzilli, R. O. Pohl, and J. W. Vandersande, *J. Phys. Chem. Solids* **48**, 641 (1987).
[77] A. V. Virkar, T. B. Jackson, and R. A. Cutler, *J. Am. Ceram. Soc.* **72**, 2031 (1989).

[78] I. Pomeranchuk, *J. Phys. USSR* **4**, 259 (1941).
[79] G. A. Slack, *Phys. Rev.* **105**, 829 (1957).
[80] T. H. Geballe and G. W. Hull, *Phys. Rev.* **110**, 773 (1958).
[81] D. G. Onn, A. Witek, Y. Z. Qiu, T. R. Anthony, and W. F. Banholzer, *Phys. Rev. Lett.* **68**, 2806 (1992).
[82] T. R. Anthony, W. F. Banholzer, J. F. Fleischer, L. Wei, P. K. Kuo, R. L. Thomas, and R. W. Pryor, *Phys. Rev. B* **42**, 1104 (1990).
[83] J. R. Olson, R. O. Pohl, J. W. Vandersande, A. Zoltan, T. R. Anthony, and W. F. Banholzer, *Phys. Rev. B* **47**, 14850 (1993).
[84] L. Wei, P. K. Kuo, R. L. Thomas, T. R. Anthony, and W. F. Banholzer, *Phys. Rev. Lett.* **70**, 3764 (1993).
[85] T. Ruf, R. W. Henn, M. Asen-Palmer, E. Gmelin, M. Cardona, H.-J. Pohl, G. G. Devyatych, and P. G. Sennikov, *Solid St. Commun.* **115**, 243 (2000).
[86] T. Ruf, R. W. Henn, M. Asen-Palmer, E. Gmelin, M. Cardona, H.-J. Pohl, G. G. Devyatych, and P. G. Sennikov, *Solid St. Commun.* **127**, 257 (2003).
[87] K. C. Hass, M. A. Tamor, T. R. Anthony, and W. F. Banholzer, *Phys. Rev. B* **45**, 7171 (1992).
[88] R. Berman, *Phys. Rev. B* **45**, 5726 (1992).
[89] N. V. Novikov, A. P. Podoba, S. V. Shmegara, A. Witek, A. M. Zaitsev, A. B. Denisenko, W. R. Fahrner, and M. Werner, *Diamond and Related Materials* **8**, 1602 (1999).
[90] P. G. Klemens, *Proc. Roy. Soc.* **A68**, 1113 (1955).

http://www.springer.com/978-0-387-22021-5

High Thermal Conductivity Materials
Shinde, S.L.; Goela, J. (Eds.)
2006, XVIII, 271 p. 133 illus., Hardcover
ISBN: 978-0-387-22021-5